High-Performance TiN/Al_2O_3/ZnO/Al_2O_3/TiN Flexible RRAM Device With High Bending Condition

Dayanand Kumar, Umesh Chand, Lew Wen Siang, and Tseung-Yuen Tseng, *Fellow, IEEE*

***Abstract*— The bipolar resistive switching (RS) characteristics of the ZnO-based TiN/Al_2O_3/ZnO/Al_2O_3/TiN structure are investigated for flexible nonvolatile memory applications. Using a thin Al_2O_3 buffer layer on both sides of the ZnO device shows uniform and eminently stable bipolar resistance switching characteristics. The device exhibits good RS with more than two orders of resistance ON-OFF ratio, retention of $>10^4$ s at 120 °C, good dc endurance $>10^4$ cycles, and high ac endurance of $>10^8$ cycles with 40-ns pulsewidth without any degradation. The device shows high mechanical stability when under 10^4 continuous repetitive flexible bendings, indicating that high endurance with a very small bending radius of up to 3 mm. The lower Gibbs free energy of the Al_2O_3 (-1676 kJ/mol) film compared with the ZnO (-320.4 kJ/mol) and TiO_2 (-994 kJ/mol) films can improve the RS properties of the TiN/Al_2O_3/ZnO/Al_2O_3/TiN device. The significant improvement in the TiN/Al_2O_3/ZnO/Al_2O_3/TiN device is due to the reason that thin Al_2O_3 layers on both sides of ZnO would help stabilize the local oxygen migrations for the formation and rupture of the conductive filament during the continuous switching cycles, resulting in high memory switching characteristics.**

***Index Terms*— Conductive filament (CF), Gibbs free energy, Poole–Frenkel conduction, resistive switching (RS).**

I. Introduction

THE nonvolatile resistive random access memory (RRAM) is one of the most prominent candidates for nonvolatile memory applications because of its excellent scaling ability, good reliability, robust switching speed, and very strong capability for the CMOS process [1]–[5]. In recent years, flexible substrate-based devices are very promising and essential due to their lightweight, being globally friendly, and low cost, for various applications in flexible displays, transistor, diodes, touch panel devices, as well as integrated circuits. However, lack of good performance is the major issue in the flexible substrate-based devices for future memory applications [6], [7]. To achieve excellent RRAM characteristics, various studies have been performed to investigate the resistive switching (RS) phenomenon in distinct materials [8]. Metal oxides such as TaO_x, Al_2O_3, ZrO_2, TiO_2, SiO_x, and ZnO, in particular, have received more attention for their use in fabricating RRAMs because of their good compatibility with semiconductor technologies and low-cost fabrication [9]–[17]. Among these materials, ZnO has promising characteristics such as excellent RS properties, large breakdown electric field, better endurance, and good thermal stability [15]. So far, various models have been proposed to explain the RS phenomenon of the RRAM, including the conductive filament (CF) model. The growth and annihilation of CFs in oxides were widely accepted to explain the RS phenomenon. The wide variety of experimental results reported in the literature proved the presence of CFs [2], [3]. However, the stochastic formation and rupture of the CFs cause the fluctuation in the RS properties during continuous switching cycles, which may lead to severe control and readout problems. Based on the previous studies, the RRAM device would be highly stable and reliable for practical applications, if the regions where the formation and rupture of the CFs occur can be controlled, such as inserting a thin layer between the electrode and the RS layer is one of the best ways to confine the region where the filament is formed to improve the switching characteristics of the RRAM [18], [19]. Kim *et al.* [18] have shown that a thin IrO_2 layer, inserted on both sides of the NiO film reduced the fluctuation in the switching parameters by stabilizing the local oxygen migrations for filament formation and rupture. According to the RS mechanisms, Chen *et al.* [19] reported more stable and reliable RRAM for practical applications by inserting thin Al_2O_3 layers between NbAlO films and electrodes. Other studies also showed that inserting a thin Al_2O_3 layer in between the HfO_2 switching layer and the metallic bottom electrode (BE) allowed improving the memory window as well as the operating current [20], [21].

Manuscript received November 8, 2019; accepted December 10, 2019. Date of publication January 13, 2020; date of current version January 27, 2020. This work was supported by National Science Council, Taiwan, under Project NSC 105-2221-E-009-134-MY3. The review of this article was arranged by Editor T. Kim. *(Corresponding authors: Lew Wen Siang; Tseung-Yuen Tseng.)*

D. Kumar is with the Institute of Electronics, National Chiao Tung University, Hsinchu 300, Taiwan, and also with the School of Physical and Mathematical Sciences, Nanyang Technological University, Singapore 637371.

U. Chand is with the Electrical and Computer Engineering, National University of Singapore, Singapore 119077.

L. W. Siang is with the School of Physical and Mathematical Sciences, Nanyang Technological University, Singapore 637371 (e-mail: wensiang@ntu.edu.sg).

T.-Y. Tseng is with the Institute of Electronics, National Chiao Tung University, Hsinchu 300, Taiwan (e-mail: tseng@cc.nctu.edu.tw).

Color versions of one or more of the figures in this article are available online at http://ieeexplore.ieee.org.

Digital Object Identifier 10.1109/TED.2019.2959883

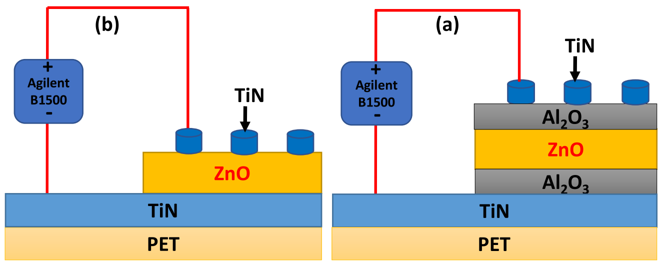

Fig. 1. Schematics of (a) TiN/ZnO/TiN and (b) TiN/Al_2O_3/ZnO/Al_2O_3/TiN devices, respectively.

In this article, in order to evaluate the memory cell for flexible technologies and to project for future flexible 1T1R monolithic technology, we have investigated the high performance of a low-temperature, ZnO-based memory device with the insertion of thin Al_2O_3 buffer layers at the interfaces of the top and bottom of the ZnO film in the TiN/Al_2O_3/ZnO/Al_2O_3/TiN device, which have not been achieved before. Such an arrangement can reduce the fluctuations in the switching parameters by stabilizing the local oxygen migrations for filament formation and rupture. Besides, the lower Gibbs free energy of the thin Al_2O_3 layer compared with TiO_2 and ZnO can improve the RS characteristics of the devices.

II. Experiment

The fabrication process of the devices is initiated with the cleaning of the flexible polyethylene terephthalate (PET) substrate. First, a 100-nm TiN BE was deposited on the PET substrate by sputtering technique at room temperature (RT). A thin 3-nm Al_2O_3 film was deposited on TiN BE by RF-sputtering at RT under 5-mTorr pressure with an Ar/O_2 mixture gas ratio of 10:3 SCCM. Then, a 9-nm thick ZnO film was deposited on the Al_2O_3 layer by RF sputtering at RT under working pressure (10 mTorr) and Ar/O_2 gas flow (2:1 SSCM). After that, a 3-nm thick Al_2O_3 layer was also deposited by RF-sputtering on top of the ZnO layer under 5-mTorr pressure and an O_2 gas flow of 10 SSCM to reduce the amount of oxygen vacancies in the Al_2O_3 layer. Finally, a 100-nm TiN top electrode (TE) with a diameter of 100 μm using a metal shadow mask was deposited by sputtering at RT to form the TiN/Al_2O_3/ZnO/Al_2O_3/TiN device. For comparison, a TiN/ZnO/TiN single layer structure without the Al_2O_3 layer was also fabricated. The dc electrical measurements were performed by using an Agilent B1500A semiconductor parameter analyzer, and the ac pulse was generated by an Agilent B1530A waveform generator/fast measurement unit (WGFMU). The voltage was applied on the TiN TE with the TiN BE grounded.

III. Results and Discussion

Fig. 1(a) and (b) shows the schematic of the TiN/ZnO/TiN and TiN/Al_2O_3/ZnO/Al_2O_3/TiN devices, respectively. The forming process is required for both the fresh devices to initiate the RS. Fig. 2(a) and (c) presents the typical forming behaviors for the ZnO- and Al_2O_3-based devices, where forming voltages are around 4.2 and 5 V, respectively, in which

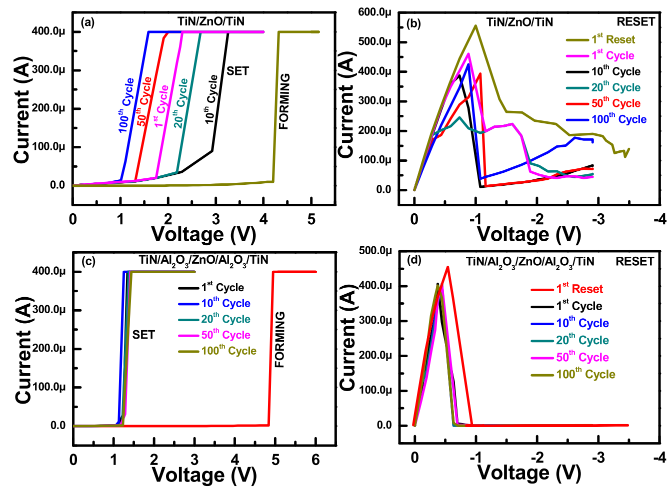

Fig. 2. (a) I–V curves of the forming and repetitive set processes with larger dispersion in the set voltage in the ZnO-based device. (b) I–V curves of the reset processes when applying a negative voltage sweep in the ZnO-based structure. (c) and (d) Narrow dispersion of the set and reset processes in the Al_2O_3-based device.

400-μA current compliance is required to protect the devices from permanent dielectric breakdown. Because the wide conductive path forms during the forming process under a high bias voltage, the first reset process of the I–V curve shows a larger current and voltage than the following reproducible reset cycles. A relatively lower resistance is also observed during the first reset process than the low resistance state (LRS) in the successive set operations. This should be a result of the parasitic capacitance on the device, which discharges through the filament during the forming or set process [19]. The voltage distributions of the SET and RESET processes, in the case of repetitive dc switching cycles, can be observed from Fig. 2. Compared to the SET and RESET processes of the ZnO device, as shown in Fig. 2(a) and (b), smaller dispersions in the values of the SET and RESET voltages are found along with the highly uniform, repetitive SET and RESET processes of the Al_2O_3-based device, as shown in Fig. 2(c) and (d).

The wide variation in the SET/RESET voltages is attributed to the random formation and rupture of CFs in the ZnO-based device, while the effective RS region is confined in the Al_2O_3-based device, so that the device possesses low operation voltages and sharp distributions of SET and RESET, leading to stable RS characteristics. Introducing a thin Al_2O_3 layer on both sides of the ZnO layer greatly enhances the switching properties of the Al_2O_3 device, where SET/RESET voltages and LRS/high resistance state (HRS) are more stable than ZnO-based devices. The dc endurance characteristics of the ZnO- and Al_2O_3-based devices are shown in Fig. 3. The dc endurance of the ZnO devices is stable up to 200 cycles only, while the insertion of a thin Al_2O_3 layer on both sides of ZnO greatly enhances the switching cycles for more than 10^4 cycles, as shown in Fig. 3(a) and (b), respectively. The HRS degradation is more severe [Fig. 3(a)], which is caused by the defects or oxygen vacancies that can be easily generated inside the switching layer, due to thermal joule heating. Therefore, the HRS is not stable, because the oxygen

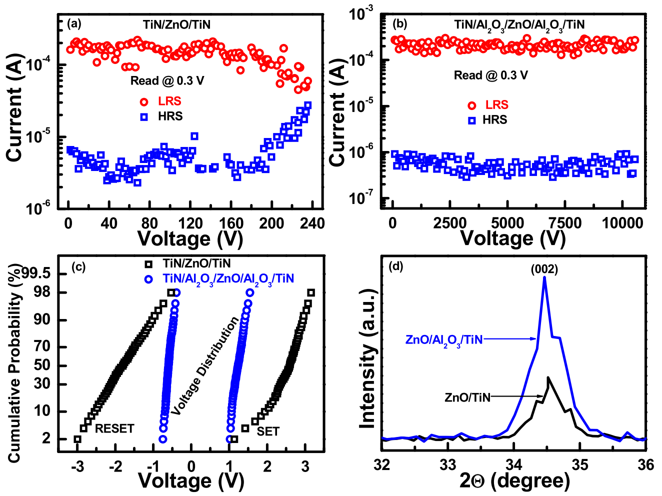

Fig. 3. (a) DC endurance of the ZnO-based device. (b) DC endurance of the Al_2O_3-based device. (c) Voltage distribution of ZnO- and Al_2O_3-based devices. (d) XRD data on ZnO deposited on TiN and Al_2O_3/TiN.

vacancies can randomly generate in the switching layer, which will link together and try to form a conductive filament. Hence, the device gradually transits its state from HRS to LRS [22]. The distributions of voltages for the ZnO- and Al_2O_3-based devices analyzed at a read voltage of 0.3 V during 100 continuous dc switching cycles are plotted in Fig. 3(c). The wider fluctuations in the SET/RESET voltages of the ZnO-based device as compared to those of the Al_2O_3-based device are attributed to the stochastic formation and rupture of CFs in the ZnO device, while the effective RS region is confined in the Al_2O_3 device, so that the device retains sharp distributions of SET/RESET voltages, leading to highly stable switching characteristics. Fig. 3(d) depicts the X-ray diffraction (XRD) spectra of ZnO with and without a thin Al_2O_3 layer on TiN BE to confirm the reason for the memory switching stability by the Al_2O_3 thin inserting layer. The XRD spectra of devices were measured in a grazing incidence mode. The peak intensity of ZnO with Al_2O_3 is increased more than two times, as compared to that without Al_2O_3. This indicates an enhancement of crystallinity compared with ZnO on TiN. This suggests that more crystallized ZnO will help to stabilize the memory switching characteristics. It is consistent with empirical observations that the memory switching would become more stable as the ZnO crystallinity increases [18]. According to the conductive filament model, conductive filaments can easily grow along the grain boundaries. It is well known that ZnO has polycrystalline nature (In fact, based on previous experience, we can say that it easily forms the (002) preferred orientation grain, so that most of the grain boundaries are perpendicular to the substrate.), and grains are formed during the growth of polycrystalline ZnO. Hence, as a result of grain boundaries, conductive filaments would form and rupture along the grain boundaries of the ZnO layer, causing stabilization in both the HRS and LRS of the RRAM devices [23].

Fig. 4(a) and (b) shows the cycle-to-cycle and device-to-device uniformity of the LRS and HRS values for different devices. The distribution is wider for the ZnO-based devices compared to that of the Al_2O_3-based devices. This wider

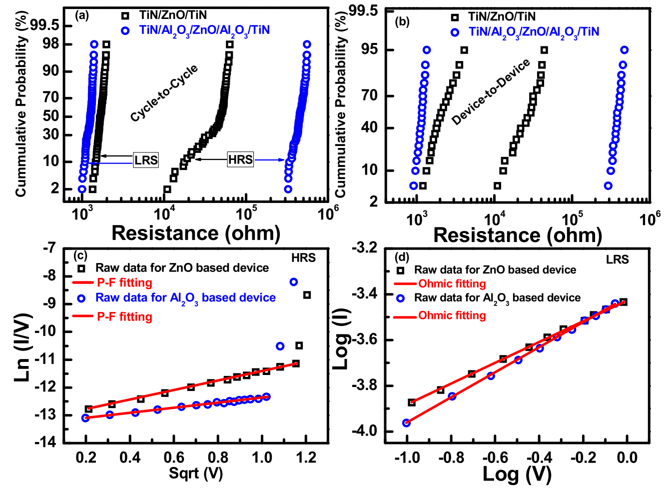

Fig. 4. (a) and (b) Distribution of the cycle-to-cycle and device-to-device variations of the LRS and HRS values for different devices, respectively. (c) P–F fitting of the *I*–*V* characteristics of both ZnO- and Al_2O_3-based devices in the HRS. (d) Linear fitting of the *I*–*V* characteristics of both devices in the LRS.

distribution in the LRS and HRS values for the ZnO-based device can be attributed to the possibility of higher leakage paths due to higher oxygen vacancies in ZnO, causing fluctuations in the LRS/HRS during different switching cycles. The small variation of the LRS/HRS values in the Al_2O_3-based device represents the high stability of the devices for their nonvolatile memory application in near future. In order to clarify the conduction mechanism, the I–V curves are fit by Poole–Frenkel (P–F) fitting according to the linear relationship between ln (I/V) and the square root of the applied voltage $(V^{1/2})$ in the HRS, as shown in Fig 4(c). The I–V curves are fit well representing the presence of P–F conduction for ZnO- and Al_2O_3-based devices. In the LRS, the conduction mechanism of the curves representing the Ohmic conduction for both the devices is shown in Fig. 4(d). In the HRS, the electrons can pass through the oxygen vacancies presented in the devices causing P–F type of conduction. In the LRS, the current flows through the filament formed by the oxygen vacancies in the devices resulting in Ohmic conduction of the electrons through the devices.

Fig. 5 depicts the X-ray photoelectron spectra (XPS) of both the devices. The O 1s spectra of the ZnO and Al_2O_3 layers can be deconvoluted into two peaks shown in Fig. 5(a) and (b), respectively. The lower binding energies of the O 1s peak at around 529.9 and 531.4 eV correspond to the Zn–O and Al–O bonding in ZnO and Al_2O_3 layers, respectively, while slightly higher energies of 532.1 and 532.2 eV in the O 1s spectra are attributed to the oxygen vacancies in ZnO and Al_2O_3 layers, respectively [15], [24], [25]. The concentrations of oxygen vacancies for ZnO and Al_2O_3 layers are about 40% and 10%, respectively. The XPS depth profile of the Al_2O_3/ZnO/Al_2O_3 structure is analyzed, as shown in Fig. 5(c). All layers can be recognized easily with different colors. Fig. 5(d) also represent the oxygen vacancy concentration of the TiN/Al_2O_3/ZnO/Al_2O_3/TiN device. The highest oxygen vacancy concentration of about 40% for the ZnO RS layer is observed. The underlying Al_2O_3-interface layer near the TiN BE has an oxygen vacancy concentration of about

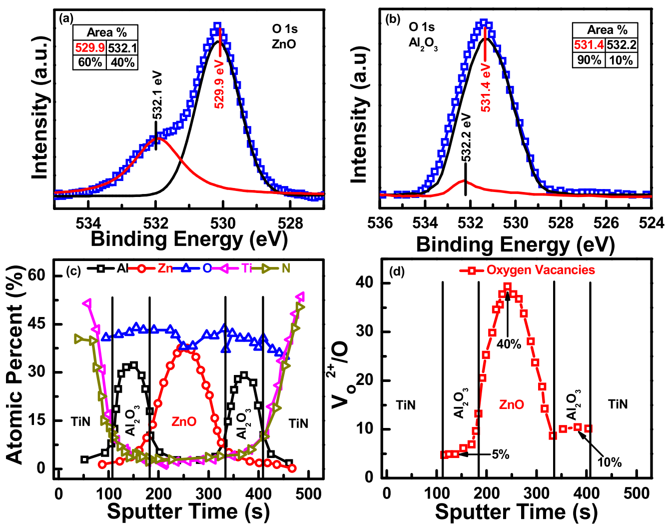

Fig. 5. O 1s XPS spectra of (a) ZnO and (b) Al_2O_3 thin films. (c) XPS depth profiles of the TiN/Al_2O_3/ZnO/Al_2O_3/TiN device. (d) Distribution of oxygen vacancy concentration of layers in the TiN/Al_2O_3/ZnO/Al_2O_3/TiN device.

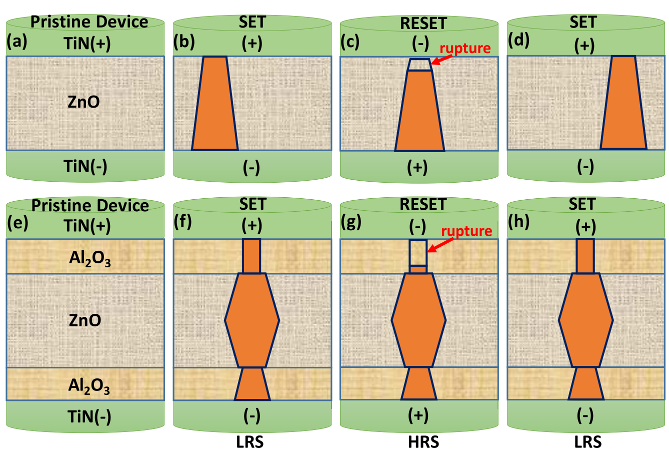

Fig. 6. (a)–(d) Schematic of random formation and rupture of the CF in the TiN/ZnO/TiN device. (e)–(h) Schematic of the formation and rupture of the CF in the TiN/Al_2O_3/ZnO/Al_2O_3/TiN device.

10%, which is higher than that of the upper Al_2O_3-interface layer (5%) [2], [26]. The oxygen vacancies play an important role in constructing the CFs in the ZnO and Al_2O_3 layers. Higher oxygen vacancies in the layer construct thicker filaments, which is discussed in the CF filament model.

According to the CF model, the wider fluctuations in the RS parameters can be controlled by stabilizing the formation and rupture of the CF during continuous switching cycles. The formation and rupture of the CF occurs at a certain portion near the metal oxide interfaces in the ZnO- and Al_2O_3-based devices. Fig. 6(a) and (d) shows the schematics of the formation and rupture of CFs for the ZnO-based device. The CFs form into a conical shape, where the thicker part of the filament is on the cathode side while the thinner part is on the anode side [27], [28]. Therefore, during the forming process, the RS region is feasibly closer to the interface of TiN TE and the RS layer in the ZnO device, as illustrated in Fig. 6(b). When a positive voltage is applied to the TiN TE, oxygen vacancies are generated in the ZnO layer and migrate toward the TiN BE to form conical shape filaments [15], [29]–[31]. The device switches from the initial resistance state to the LRS. When the negative voltage is applied on the TiN TE, oxygen ions drift easily from TiN TE to recombine with the oxygen vacancies due to the high mobility of oxygen ions along the grains boundaries, resulting in the rupturing of filaments at the TiN TE/ZnO interface, as shown in Fig. 6(c). Next, on application of a positive voltage on TiN, the device switches back to the LRS during the set process, as shown in Fig. 6(d). However, when the RS occurs near the TE interface, loss of oxygen from TE along the grain boundaries degrades the device performance [15]. This phenomenon is due to that no sufficient oxygen ions could recombine with oxygen vacancies for rupturing the conducting filaments (CF). Hence, this phenomenon leads to shrinking of the ratio (ON/OFF ratio) between the LRS and the HRS during RS cycles and causes the endurance degradation problem [32], [33]. Therefore, the poor endurance up to 240 cycles and a small resistance ratio are found in the ZnO-based device. Conversely, the formation and rupture of CF in the Al_2O_3-based device are shown in Fig. 6(e)–(h). During the forming process, oxygen vacancies are generated and they move toward the TiN BE, while the oxygen ions move toward the TiN TE to form the CF, which is narrower on both sides of the Al_2O_3 layers and thicker in the ZnO layer due to higher oxygen vacancies in the ZnO layer than in Al_2O_3 layers [34]–[37]. The device switches from the HRS to the LRS, as shown in Fig. 6(f). During the reset process, when a negative voltage is applied on TiN TE, oxygen ions return from TiN TE and recombine with the oxygen vacancies. The filament ruptures at the weakest part, which is located at the upper Al_2O_3 layer due to the effect of local Joule heating, and the device switches from the LRS to the HRS, as indicated in Fig. 6(g). In addition, during the set process, the device switches from the HRS to the LRS, with the drifting of the oxygen ions toward TiN TE for the reconstruction of the CF, as shown in Fig. 6(h). In contrast, the CF would be constructed in the RS layer in the ZnO-based device due to the generation of oxygen vacancies with the application of a high electric field [18]–[21]. The thin Al_2O_3 interface layer can be used to stabilize the formation and rupture of the CF in the Al_2O_3-based device, indicating highly stable switching performance. On the other hand, the Al_2O_3-based device shows excellent RS compared to the ZnO-based device. This phenomenon indicates that less oxygen vacancies are generated in the Al_2O_3-based device than those in the ZnO one [Fig. 5(d)]. The higher oxygen vacancy generation in ZnO causes the higher leakage current, which decreases the LRS/HRS ratio and endurance characteristics of the ZnO-based device [4]. The Al_2O_3-based device reveals a larger LRS/HRS ratio during RS [20]. This is because Al_2O_3 is a highly stable material with high thermal stability. Furthermore, Al_2O_3 has a lower Gibbs free energy (−1676 kJ/mol) than ZnO (−320.4 kJ/mol) [38], [39]. Materials with a lower Gibbs free energy are more stable compared to those with higher Gibbs free energy materials.

The mechanical stability is also investigated for the Al_2O_3-based device for its flexible applications. The LRS/HRS

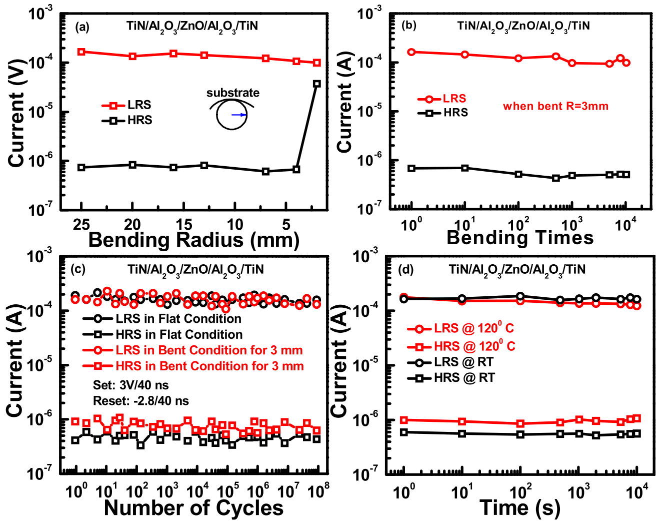

Fig. 7. (a) Memory window of the TiN/Al_2O_3/ZnO/Al_2O_3/TiN device with different bending radii. (b) Endurance characteristics of the TiN/Al_2O_3/ZnO/Al_2O_3/TiN device after continuous bending at R = 3 mm. (c) AC endurance test for the TiN/Al_2O_3/ZnO/Al_2O_3/TiN device. (d) Retention test of the Al_2O_3-based device at RT and 120 °C.

values of the device is measured at the read voltage of 0.3 V with different bending radii starting from the flat condition (25 mm) to the bending condition (2 mm), as shown in Fig. 7(a). The device shows a very stable LRS/HRS ratio without any degradation of the bending up to 3 mm and degrades rapidly at a bending radius of 2 mm. The degradation in the resistances of the device during a bending radius of 2 mm [Fig. 7(a)] may be attributed to the increase of the sheet resistance of the RS layer and BE during the bending condition [25], [40]–[42]. Fig. 7(b) exhibits the mechanical stability of the Al_2O_3-based device during the continuous 10^4 times repetitive bendings with the bending radius of 3 mm, indicating that both LRS/HRS are highly stable without any degradation. To test the reliability of the device, the ac endurance property was measured at the flat and bending condition and the results are shown in Fig. 7(c). The Al_2O_3 device can well maintain its both LRS/HRS states more than 10^8 cycles without any degradation with the LRS/HRS ratio of more than two orders of magnitude at the read voltage of 0.3 V. The retention properties of the device are also measured in the LRS and the HRS at RT and 120 °C, as depicted in Fig. 7(d), indicating stable retention characteristics for more than 10^4 s with the stable LRS/HRS ratio of about two orders of magnitude without any degradation making it well suitable for future flexible memory device applications.

To confirm why the Al_2O_3-based device gives the high performance, we further investigated the RRAM characteristics of the TiN/TiO_2/ZnO/TiO_2/TiN flexible device for comparison. The RS characteristics of the TiO_2-based device is shown in Fig. 8(a). The device exhibits the bipolar resistive switching (BRS) behavior with a low resistance ratio than the Al_2O_3-based device, which confirms the higher leakage current in the TiO_2-based device due to the generation of more oxygen vacancies, as compared to the Al_2O_3-based device. Fig. 8(b) depicts the dc endurance characteristic of the TiO_2-based device in comparison with that of the Al_2O_3-based device. Obviously, the TiO_2-based device maintained its original states up to 7000 cycles without any degradation, but with inferior performance than Al_2O_3 one. The Al_2O_3-based device exhibits a higher LRS/HRS ratio during switching compared to the TiO_2-based device. This phenomenon is probably due to the lower Gibbs free energy of Al_2O_3. The standard Gibbs free energies for Al_2O_3 and TiO_2 are -1676 kJ/mol and -994 kJ/mol at RT, respectively [43]–[46]. The higher Gibbs free energy value of TiO_2 than Al_2O_3 indicates that the TiO_2-based device generates higher concentration of oxygen vacancies causing higher leakage current. Therefore, the Al_2O_3-based device shows a higher performance than TiO_2- and ZnO-based devices.

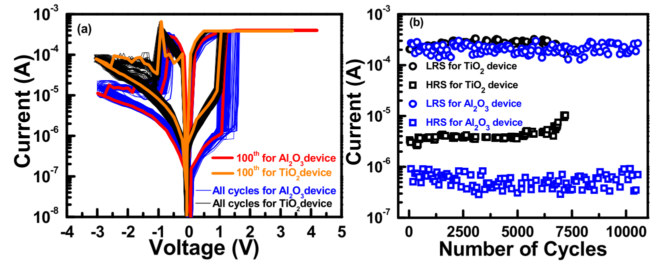

Fig. 8. (a) RS curves of Al_2O_3- and TiO_2-based devices. (b) DC endurances of TiO_2- and Al_2O_3-based devices.

IV. Conclusion

In this article, the switching characteristics and uniformity of the Al_2O_3-based memory device enhanced with inserting a thin Al_2O_3 layer on both sides of ZnO were investigated. According to the CF model where the switching is associated with the formation and rupture of CF at the thin Al_2O_3-interface layer, such an Al_2O_3 layer helps to stabilize the local oxygen migration for the formation and rupture of filaments. This leads to enhanced switching performances, such as high resistance ratio ($>10^2$), endurance ($>10^4$ cycles), ac endurance ($>10^8$ cycles), and stable retention at high temperatures (120 °C), achieved in the Al_2O_3-based device.

References

[1] T. Y. Tseng and S. M. Sze, *Nonvolatile Memories: Materials, Devices and Applications*, vol. 1. Los Angeles, CA, USA: American Scientific, 2012, pp. 1–9.

[2] J. J. Yang, D. B. Strukov, and D. R. Stewart, “Memristive devices for computing,” *Nature Nanotechnol.*, vol. 8, no. 1, pp. 13–24, Jan. 2013.

[3] D. Kumar, R. Aluguri, U. Chand, and T.-Y. Tseng, “Conductive bridge random access memory characteristics of SiCN based transparent device due to indium diffusion,” *Nanotechnology*, vol. 29, no. 12, Mar. 2018, Art. no. 125202.

[4] D. Kumar, R. Aluguri, U. Chand, and T.-Y. Tseng, “Enhancement of resistive switching properties in nitride based CBRAM device by inserting an Al_2O_3 thin layer,” *Appl. Phys. Lett.*, vol. 110, no. 20, May 2017, Art. no. 203102.

[5] D. Kumar, R. Aluguri, U. Chand, and T. Tseng, “Metal oxide resistive switching memory: Materials, properties and switching mechanisms,” *Ceram. Int.*, vol. 43, pp. S547–S556, Aug. 2017.

[6] D. Kumar, R. Aluguri, U. Chand, and T.-Y. Tseng, “One bipolar selector–one resistor for flexible crossbar memory applications,” *IEEE Trans. Electron Devices*, vol. 66, no. 3, pp. 1296–1301, Mar. 2019.

[7] J. Shang *et al.*, “Thermally stable transparent resistive random access memory based on all–oxide heterostructures,” *Adv. Funct. Mater.*, vol. 24, no. 15, pp. 2171–2179, Apr. 2014.

[8] A. Sawa, “Resistive switching in transition metal oxides,” *Mater. Today*, vol. 11, no. 6, pp. 28–36, Jun. 2008.

[9] T. Breuer, A. Siemon, E. Linn, S. Menzel, R. Waser, and V. Rana, "Low-current operations in 4F2-compatible Ta_2O_5-based complementary resistive switches," *Nanotechnology*, vol. 26, no. 41, Oct. 2015, Art. no. 415202.

[10] Y. Li, P. Yuan, L. Fu, R. Li, X. Gao, and C. Tao, "Coexistence of diode-like volatile and multilevel nonvolatile resistive switching in a ZrO_2/TiO_2 stack structure," *Nanotechnology*, vol. 26, no. 39, Oct. 2015, Art. no. 391001.

[11] S.-W. Yeom *et al.*, "Highly flexible titanium dioxide-based resistive switching memory with simple fabrication," *Appl. Phys. Exp.*, vol. 7, no. 10, Oct. 2014, Art. no. 101801.

[12] C.-Y. Lin, C.-Y. Wu, C.-Y. Wu, C. Hu, and T.-Y. Tseng, "Bistable resistive switching in Al_2O_3 memory thin films," *J. Electrochem. Soc.*, vol. 154, pp. G189–G192, Jul. 2007.

[13] J. Yao *et al.*, "Highly transparent nonvolatile resistive memory devices from silicon oxide and graphene," *Nature Commun.*, vol. 3, no. 1, p. 1101, Jan. 2012.

[14] T.-L. Tsai, H.-Y. Chang, J. J.-C. Lou, and T.-Y. Tseng, "A high performance transparent resistive switching memory made from ZrO_2/AlON bilayer structure," *Appl. Phys. Lett.*, vol. 108, Apr. 2016, Art. no. 153505.

[15] F. M. Simanjuntak, D. Panda, T.-L. Tsai, C.-A. Lin, K.-H. Wei, and T.-Y. Tseng, "Enhanced switching uniformity in AZO/ZnO_{1-x}/ITO transparent resistive memory devices by bipolar double forming," *Appl. Phys. Lett.*, vol. 107, Jul. 2015, Art. no. 033505.

[16] J. T. Qiu, S. Samanta, M. Dutta, S. Ginnaram, and S. Maikap, "Controlling resistive switching by using an optimized MoS_2 interfacial layer and the role of top electrodes on ascorbic acid sensing in TaO_x-based RRAM," *Langmuir*, vol. 35, pp. 3897–3906, Feb. 2019.

[17] S. Samanta, S. Maikap, A. Roy, S. Jana, and J.-T. Qiu, "Effects of W/Ir top electrode on resistive switching and dopamine sensing by using optimized TaO_x-based memory platform," *Adv. Mater. Interfaces*, vol. 4, Nov. 2017, Art. no. 1700959.

[18] D. C. Kim, M. J. Lee, S. E. Ahn, S. Seo, J. C. Park, and I. K. Yoo, "Improvement of resistive memory switching in NiO using IrO_2," *Appl. Phys. Lett.*, vol. 88, Jun. 2006, Art. no. 232106.

[19] L. Chen *et al.*, "Highly uniform bipolar resistive switching with Al_2O_3 buffer layer in robust NbAlO-based RRAM," *IEEE Electron Device Lett.*, vol. 31, no. 4, pp. 356–358, Mar. 2010.

[20] L. Goux *et al.*, "Ultralow sub-500 nA operating current high-performance TiN\$Al_2O_3$\$HfO_2$\Hf\TiN bipolar RRAM achieved through understanding-based stack-engineering," in *Symp. VLSI Technol. Dig. Tech. Papers*, Jun. 2012, pp. 159–160, doi: 10.1109/VLSIT.2012.6242510.

[21] M. Azzaz *et al.*, "Benefit of Al_2O_3/HfO_2 bilayer for BEOL RRAM integration through 16 kb memory cut characterization," in *Proc. 45th Eur. Solid State Device Res. Conf. (ESSDERC)*, Sep. 2015, pp. 266–269, doi: 10.1109/essderc.2015.7324765.

[22] C.-Y. Huang, Y.-T. Ho, C.-J. Hung, and T.-Y. Tseng, "Compact Ga–doped ZnO nanorod thin film for making high-performance transparent resistive switching memory," *IEEE Trans. Electron Devices*, vol. 61, no. 10, pp. 3435–3441, Oct. 2014.

[23] U. Chand, K.-C. Huang, C.-Y. Huang, C.-H. Ho, C.-H. Lin, and T.-Y. Tseng, "Investigation of thermal stability and reliability of HfO_2 based resistive random access memory devices with cross-bar structure," *J. Appl. Phys.*, vol. 117, May 2015, Art. no. 184105.

[24] P. K. Nayak, J. A. Caraveo-Frescas, Z. Wang, M. N. Hedhili, Q. X. Wang, and H. N. Alshareef, "Thin film complementary metal oxide semiconductor (CMOS) device using a single-step deposition of the channel layer," *Sci. Rep.*, vol. 4, no. 1, May 2015, Art. no. 04672.

[25] R. Aluguri, R. Sailesh, D. Kumar, and T.-Y. Tseng, "Characteristics of flexible and transparent Eu2O3 resistive switching memory at high bending condition," *Nanotechnology*, vol. 30, no. 4, Jan. 2019, Art. no. 045202.

[26] W. Zhang *et al.*, "Bipolar resistive switching characteristics of $HfO_2/TiO_2/HfO_2$ trilayer-structure RRAM devices on Pt and TiN–coated substrates fabricated by atomic layer deposition," *Nanosc. Res. Lett.*, vol. 12, no. 1, p. 393, Dec. 2017.

[27] D.-H. Kwon *et al.*, "Atomic structure of conducting nanofilaments in TiO_2 resistive switching memory," *Nature Nanotechnol.*, vol. 5, no. 2, pp. 148–153, Feb. 2010.

[28] M.-H. Lin, M.-C. Wu, C.-Y. Huang, C.-H. Lin, and T.-Y. Tseng, "High-speed and localized resistive switching characteristics of double-layer $SrZrO_3$ memory devices," *J. Phys. D, Appl. Phys.*, vol. 43, Jul. 2010, Art. no. 295404.

[29] K. M. Kim *et al.*, "Collective motion of conducting filaments in Pt/n-Type TiO_2/p-type NiO/Pt stacked resistance switching memory," *Adv. Funct. Mater.*, vol. 21, no. 9, pp. 1587–1592, May 2011.

[30] Y.-E. Syu *et al.*, "Endurance improvement technology with nitrogen implanted in the interface of $WSiO_x$ resistance switching device," *IEEE Electron Device Lett.*, vol. 34, no. 7, pp. 864–866, Jul. 2013.

[31] P. H. Chen *et al.*, "Bulk oxygen–ion storage in indium–tin–oxide electrode for improved performance of HfO_2-based resistive random access memory," *IEEE Electron Device Lett.*, vol. 37, no. 3, pp. 280–283, Mar. 2016.

[32] J. J. Yang *et al.*, "The mechanism of electroforming of metal oxide memristive switches," *Nanotechnology*, vol. 20, no. 21, May 2009, Art. no. 215201.

[33] U. Chand, C.-Y. Huang, J.-H. Jieng, W.-Y. Jang, C.-H. Lin, and T.-Y. Tseng, "Suppression of endurance degradation by utilizing oxygen plasma treatment in HfO_2 resistive switching memory," *Appl. Phys. Lett.*, vol. 106, Apr. 2015, Art. no. 153502.

[34] L.-G. Wang *et al.*, "Excellent resistive switching properties of atomic layer-deposited $Al_2O_3/HfO_2/Al_2O_3$ trilayer structures for non-volatile memory applications," *Nanosc. Res. Lett.* vol. 10, May 2015, Art. no. 135.

[35] K. Kinoshita, T. Tamura, M. Aoki, Y. Sugiyama, and H. Tanaka, "Bias polarity dependent data retention of resistive random access memory consisting of binary transition metal oxide," *Appl. Phys. Lett.*, vol. 89, Sep. 2006, Art. no. 103509.

[36] K. M. Kim, B. J. Choi, and C. S. Hwang, "Localized switching mechanism in resistive switching of atomic-layer-deposited TiO_2 thin films," *Appl. Phys. Lett.*, vol. 90, Jun. 2007, Art. no. 242906.

[37] K. M. Kim, B. J. Choi, B. W. Koo, S. Choi, D. S. Jeong, and C. S. Hwang, "Resistive switching in Pt/Al_2O_3/TiO_2/Ru stacked structures," *Electrochem. Solid-State Lett.*, vol. 9, pp. G343–G346, Sep. 2006.

[38] S. Yu, Y. Wu, Y. Chai, J. Provine, and H.-S.-P. Wong, "Characterization of switching parameters and multilevel capability in HfO_x/AlO_x bi-layer RRAM devices," in *Proc. Int. Symp. VLSI Technol., Syst. Appl.*, Apr. 2011, pp. 1–2, doi: 10.1109/vtsa.2011.5872251.

[39] U. Chand, C.-Y. Huang, and T.-Y. Tseng, "Mechanism of high temperature retention property (up to 200 °C) in ZrO_2-based memory device with inserting a ZnO thin layer," *IEEE Electron Device Lett.*, vol. 35, no. 10, pp. 1019–1021, Oct. 2014.

[40] J. Shang *et al.*, "Highly flexible resistive switching memory based on amorphous-nanocrystalline hafnium oxide films," *Nanoscale*, vol. 9, no. 21, pp. 7037–7046, Mar. 2017.

[41] Z.-W. Zheng, C.-H. Cheng, K.-I. Chou, M. Liu, and A. Chin, "Improved current distribution in resistive memory on flexible substrate using nitrogen-rich TaN electrode," *Appl. Phys. Lett.*, vol. 101, no. 24, Dec. 2012, Art. no. 243507.

[42] S.-T. Han, Y. Zhou, and V. A. L. Roy, "Towards the development of flexible non-volatile memories," *Adv. Mater.*, vol. 25, no. 38, pp. 5425–5449, Oct. 2013.

[43] J.-K. Lee *et al.*, "Accurate analysis of conduction and resistive-switching mechanisms in double-layered resistive-switching memory devices," *Appl. Phys. Lett.*, vol. 101, Sep. 2012, Art. no. 103506.

[44] L. Zhang *et al.*, "Unipolar TaO_x-based resistive change memory realized with electrode engineering," *IEEE Electron Device Lett.*, vol. 31, no. 9, pp. 966–968, Sep. 2010.

[45] W. M. Haynes, *CRC Handbook of Chemistry and Physics*, 91st ed. Boca Raton, FL, USA: CRC Press, 2010.

[46] V. Y.-Q. Zhuo *et al.*, "Improved switching uniformity and low-voltage operation in TaO_x-based RRAM using Ge reactive layer," *IEEE Electron Device Lett.*, vol. 34, no. 9, pp. 1130–1132, Sep. 2013.